


RESEARCH ARTICLE

A clinical and histopathological study of malformations observed in fetuses infected by the Zika virus

Aurélie Beaufrère¹ ; Bettina Bessières¹; Maryse Bonnière¹; Marine Driessen²; Christian Alfano³; Thérèse Couderc^{4,5}; Marc Thiry³; Nicolas Thelen³; Marc Lecuit^{4,5,6}; Tania Attié-Bitach^{1,7,8}; Michel Vekemans^{1,7,8}; Yves Ville^{2,8}; Laurent Nguyen³; Marianne Leruez-Ville^{8,9} Férechté Encha-Razavi¹

¹ Service d'Histologie-Embryologie-Cytogénétique, Hôpital Universitaire Necker-Enfants Malades, APHP, Paris, France.

² Service de Gynécologie-Obstétrique, Hôpital Universitaire Necker-Enfants Malades, APHP, Paris, France.

³ GIGA-Neurosciences, Université de Liège, Liège, Belgique.

⁴ Institut Pasteur, Biology of Infection Unit, Paris, France.

⁵ Inserm U1117, Paris, France.

⁶ Paris-Descartes University, Sorbonne Paris Cité, Centre d'Infectiologie Necker-Pasteur, Necker-Enfants Malades, Paris, France.

⁷ INSERM U-1163, Institut Imagine, Paris, France.

⁸ Université Paris Descartes, Paris, France.

⁹ Laboratoire de Virologie, Hôpital Universitaire Necker Enfants Malades, APHP, Paris, France.

Keywords

ER stress, fetus, meningoencephalitis, micrencephaly, microcephaly, ZIKV infection.

Corresponding author:

Aurélie Beaufrère, MD, Service d'Histologie-Embryologie-Cytogénétique, Hôpital Universitaire Necker-Enfants Malades, APHP, 149 rue de Sèvres 75015 Paris, France
(E-mail: aurelie.beaufrere@sfr.fr)

Received 14 March 2018

Accepted 20 June 2018

Published Online Article Accepted

18 July 2018

doi:10.1111/bpa.12644

Abstract

Background: The recent outbreak of Zika virus (ZIKV) infection and the associated increased prevalence of microcephaly in Brazil underline the impact of viral infections on embryo-fetal development. The aim of the present study is to provide a detailed clinical and histopathological study of the fetal disruption caused by the ZIKV, with a special focus on the associated neuropathological findings.

Methods: A detailed fetoplacental examination, as well as neuropathological and neurobiological studies were performed on three fetuses collected after pregnancy termination between 22 and 25 weeks of gestation (WG), because brain malformations associated with a maternal and fetal ZIKV infection was diagnosed.

Results: In all three cases, the maternal infection occurred during the first trimester of pregnancy. A small head was observed on the ultrasound examination of the second trimester of pregnancy and led to the diagnosis of ZIKV fetopathy and pregnancy termination. The fetal histopathological examination was unremarkable on the viscera but showed on the testis an interstitial lymphocytic infiltrate. The placenta contained a Hofbauer cells hyperplasia with signs of inflammation. Neuropathological findings included a meningoencephalitis and an *ex vacuo* hydrocephalus. Immunohistochemical studies showed the presence of T lymphocytic and histiocytic meningitis associated with an abundant cerebral astroglial and macrophagic reaction. *In situ* hybridization demonstrated, abundant ZIKV particles within the cerebral parenchyma mainly in the ventricular/subventricular zone and in the cortical plate. In addition massive cells death and endoplasmic reticulum damage were present.

Conclusion: The present study reports on the clinical and histopathological findings observed in three fetuses infected by the ZIKV. It emphasizes the severity of brain damages and the minimal visceral and placental changes observed upon ZIKV infection. This confirms the selective neurotropism of ZIKV. Finally, it allows us to describe the cascade of multifactorial developmental defects leading to microcephaly.

INTRODUCTION

ZIKA virus (ZIKV) is an arbovirus belonging to the *Flavivirus* genus (*Flaviviridae* family) mainly transmitted by *Aedes aegypti* mosquitoes. It was originally isolated from a sentinel primate in Uganda in 1947 (5,12,22,24). Since 2007, ZIKV infection spreads to Micronesia (2007), French Polynesia

(2013) and more recently to South America, notably to Brazil (2015–2016) (3,5,12). In humans, ZIKV is known to cause a mild febrile disease, headache, arthralgia and myalgia, a maculopapular rash and Guillain-Barre syndrome. The recent emergence of ZIKV in Brazil has been associated with an acute and significant increased prevalence of

congenital microcephaly in the 2015–2016 period (5,6,22). Cauchemez *et al* estimated that the number of microcephaly cases associated with ZIKV was 95 per 10 000 women infected during the first trimester (9). In this context, WHO declared on 1st February 2016 that ZIKV infection was a public health emergency of international concern (39).

This large outbreak has revealed that, beside mosquito transmission, ZIKV is also transmitted through hematogenic and sexual routes (5,9,24). Unlike other mosquito-borne *Flaviviruses*, ZIKV persists in human fluids for up to 6 months (24). Fetal contamination is considered to be hematogenic. The diagnosis of fetal infection is based on ZIKV RNA detection in the amniotic fluid of pregnant women, having a positive result on blood testing (serologic and/or RT-PCR testing) (12).

Affected newborns present with a syndrome characterized by a small head (microcephaly) with joint deformities (arthrogryposis). Brain imaging usually detects a small brain (micrencephaly) with ventriculomegaly, a malformed cortex, an abnormal corpus callosum and diffuse calcifications in the subcortical parenchyma and the thalamus (18,22,31). Despite the extent of the ZIKV fetal epidemics and the WHO recommendation, postmortem studies are still scarce. Indeed, only a small number of postmortem studies have been reported in infants who may have suffered from additional stress due to delivery or resuscitation attempts (11,12,22). In unborn babies, description of visceral and brain anomalies is usually based on ultrasound findings alone, whereas histopathological and neurobiological examinations are instrumental to describe in details the spectrum of lesions associated with the ZIKV infection.

The aim of the present report is precisely to better characterize the spectrum of fetal disruption caused by the ZIKV infection, by providing autopsy results with detailed visceral histopathological, neuropathological and complementary studies including immunohistochemical and neurobiological investigations.

MATERIAL AND METHODS

Population

The study concerns three fetuses collected during the January–December 2016 period and autopsied in our laboratory after a pregnancy termination was performed because brain malformations were diagnosed in a context of ZIKV maternal infection.

ZIKV infection

The detection of the ZIKV was performed using RT-PCR (RealStar[®] Zika Virus RT PCR kit 1.0 Altona, Joué-les-Tours, France) following manufacturer instructions. RNA was extracted from 200 µL of maternal plasma, amniotic fluid and fetal blood or from fetal tissues and 8 placental biopsy samples using the NucliSens[®] EasyMag[®] kit following manufacturer instructions (BioMérieux, Marcy L'étoile, France). Elution of extracted RNA was done in 100 µL

of elution buffer. The kit did not include quantification standards but allowed to perform a semi-quantitative estimation of the results based on the cycle threshold value (CT) obtained for each sample. Samples with a CT value between 35 and 40, 30 to 34, 25 to 29 and <25 were graded respectively as low positive (+), moderately positive (++), highly positive (+++) and very highly positive (++++).

Fetal autopsy

Fetal autopsy was performed after parental consent, following the guidelines of the French Society of Foetopathology (SOFFOET). It included fetal photographs and X-rays, external macroscopic examination, complete autopsy with visceral sampling for histopathological studies. Macroscopic analysis and sampling of the placenta, membranes and cord were performed after formalin fixation. Complementary samplings for viral, electron microscopy, genetic, and neurobiological studies were performed on fresh central nervous system.

Biometrical parameters were compared with published normograms established according to the gestational age (17). In Case 1, cerebral hemispheres were separated, one frozen at –80° and the other fixed in formalin zinc solution. In Cases 2 and 3, brains were fixed *in toto* after samples from the frontal and occipital horns were frozen at –80°. For histopathological studies, specimens were taken from frontal, parietal, temporal and occipital lobes, deep brain nuclei, brainstem, cerebellum, spinal cord, eyes and muscles. Histological preparations were stained with H&E and immuno-stained according to standard protocols using a panel of antibodies to explore the inflammatory response (CD3, CD20, CD45, CD68), the endothelial cells (CD34) and brain reactive astrocytosis (GFAP).

Neurobiological study

Cryosectioning

Samples from cerebral hemispheres, fixed 2 weeks in zinc formalin solution were cryoprotected (30% sucrose in PBS o.n.) before embedding in NEG-50 Blue (Thermo Scientific) for cryosectioning (Leica) (20µm) onto slides (SuperFrost Plus, 326 VWR International).

RNA *in situ* hybridization (ISH)

Non-radioactive RNA *in situ* hybridizations using digoxigenin-labeled sense and antisense riboprobes for hCHOP and ZIKV mRNA were performed on frozen fresh cerebral hemispheric sections as described previously (8). The templates were: (i) a PCR fragment amplified from hCHOP complete sequence (cDNA clone MGC:4154, IMAGE:330545 from Source Bioscience LifeSciences) and cloned in a PCR-II TOPO vector (Thermo Fisher Scientific) according to manufacturer instructions; (ii) a PCR fragment amplified from the ZIKV genome (GCF_000882815.3). The following primers were used to amplify the 3'UTR region of hCHOP and ZIKV cDNAs:

CHOP.FW 5'-AATCTTCACCACTCTTGACCCTGC -3',
 CHOP.REV 5'-CTTTTGTCTACTCCAAGCCTTCCC -3',
 ZIKV.FW 5'-AGGTGAAGCACGGAGATCTAGAAG -3',
 ZIKV.REV 5'-CCACTAACGTTCTTTTGCAGACAT -3'.

The riboprobes were synthesized using the DIG labeling mix (Roche) according to manufacturer instructions.

Transmission Electron Microscopy (TEM)

Samples were fixed for 24 hours at 4°C in 2.5% glutaraldehyde in Sorensen's buffer 0.1M. After several washes in Sorensen's buffer, samples were post-fixed at 4°C with 2% osmium tetroxide in Sorensen's buffer 0.1M for 60 min, then washed in deionized water, dehydrated at room temperature through a graded ethanol series (70%, 96% and 100%) and embedded in Epon for 48 hours at 60°C. Ultrathin 70 nm sections were obtained using an ultramicrotome (Reichert Ultracut E) equipped with a diamond knife (Diatome). The sections were mounted on copper grids coated with collodion and contrasted with uranyl acetate and lead citrate for 15 minutes each. The ultrathin sections were observed under a JEM-1400 transmission electron microscope (Jeol) at 80 kV and photographed with an 11 MegaPixel bottom-mounted TEM camera system (Quemesa, Olympus). The images were analyzed using RADIUS software (Olympus).

Immunofluorescence

This was performed as described previously (38). Briefly antigen retrieval (Dako Target Retrieval Solution,) was performed at 95°C for 15 minutes, prior to incubation with primary antibodies. The primary antibody was an anti-NS1 from Dengue Virus conjugated with Alexa-546 (1:500, isolated by Marie Flamand). Nuclei were counterstained with Hoechst (1:5000, Thermo Fisher Scientific) and mounted in Mowiol (SIGMA) solution.

Imaging

Immunofluorescence pictures were visualized using the Nikon A1 confocal microscope or a Carl Zeiss LSM710 confocal microscope. *In-situ* hybridizations pictures were visualized using an Olympus AX70 PROVIS microscope.

Ethics

A parental consent was signed by the parents to participate to this research.

All procedures were approved by the ethics committee (Agence de BioMedecine, approval: PFS 15-009).

RESULTS

Here we report on the clinical and histopathological findings observed in three fetuses ascertained after pregnancy termination in the context of a maternal ZIKV infection acquired during the first trimester of pregnancy (Table 1).

Clinical data

In all three fetuses, the mother, living respectively in Martinique, Venezuela and Guadeloupe presented an episode of fever and a skin rash evocative of ZIKV infection during the first trimester of pregnancy (13 weeks of gestation (WG) in case 1; 9 WG in case 2 and 8 WG in case 3). In each case, the maternal ZIKV infection was confirmed by blood RT-PCR. The first trimester obstetrical ultrasound examination was unremarkable in all three cases. The second trimester ultrasound examination showed respectively in Case 1 at 22 WG, a moderate ventriculomegaly, calcified ventricular walls and hypoplasia of the corpus callosum; in Case 2, at 21 WG growth retardation and microcephaly with deformed lateral ventricles and in Case 3 at 20 WG hepatic calcifications and cerebral anomalies including microcephaly, a misplaced fourth ventricle, a corpus callosum agenesis, enlarged occipital ventricles with hyperechogenic walls. Amniotic fluid RT-PCR for ZIKV infection was highly positive (+++) in Cases 1 and 2 and moderately positive (++) in Case 3. RT-PCR test for ZIKV detection on fetal blood performed in Cases 2 and 3 showed a low positivity (+) in both cases. Termination of pregnancy was performed at 25 WG in Case 1 and at 22 WG in Cases 2 and 3.

Fetal examination

External macroscopic examination showed in Case 1 a female eutrophic fetus (weight: 831 g, 50th percentile for term), in Case 2 a male fetus with growth retardation (weight: 341 g, 5th percentile for term) and in Case 3 a male eutrophic fetus (weight: 374 g, 10th percentile for term). All fetuses presented a small head. None had joint deformity.

Visceral examination

Hepatomegaly (enlarged liver weight: 63 g, >95th percentile for term), splenomegaly (enlarged spleen weight: 11.6 g, >95th percentile for term) and thymus hypertrophy (thymus weight: 6 g, >95th percentile for term) were observed in Case 1. In Case 2, adrenal gland hypoplasia (adrenals weight: 0.4 g, <5th percentile for term) was observed. No internal anomaly was noted in Case 3. Microscopic examination showed no major visceral changes, except an interstitial lymphocytic infiltrate (confirmed by anti-CD45 immunohistochemistry) in the testis of both male fetuses (Fig. 1A and 1B).

Neuropathological examination

Gross examination showed small cerebral hemispheres with an hypoplastic brainstem and cerebellum, covered with congestive and thickened meninges, weighing below <5th percentile for age in Case 1 and 2 (47.3 g in Case 1, 39.8g in Case 2), and at the 10th percentile in Case 3 (47.5g). Coronal sections of cerebral hemispheres showed various degrees of ventricular dilatation and corpus callosum

Table 1. Clinical, microbiological and histopathological data of fetuses infected by ZIKV.

Case No	WG at PI	US features at amniocentesis sampling	WG Amnio-centesis/ or blood sampling	WG at Amnio-centesis/ blood sampling	PCR in maternal blood at amniocentesis	PCR in fetal blood at TOP	Sex	WG at Amnio-centesis/ or blood sampling	WG Amnio-centesis/ or blood sampling	PCR in maternal blood at amniocentesis	PCR in fetal blood at TOP	Macroscopic anomalies of fetal brain at TOP	Macroscopic anomalies of fetal brain	Microscopic anomalies of fetal brain	Anti CD68 staining in fetal brain	Anti CD3 staining in fetal brain	PCR in fetal brain	Macroscopic anomalies of other organs the placenta	Microscopic anomalies of the placenta	Zika PCR in placenta (%) positive biopsies)
1	13	Moderate ventriculomegaly	23	NA	+++	+	F	25	Hepatomegaly	Microcephaly (<5 th percentile)	Microcephaly (<5 th percentile)	Arachnoiditis Ependymitis	++	+++	++	++++	No	Hypotrophic (<5 th percentile)	Acute chorioamnionitis	++
		Atrophy of corpus callosum							Splenomegaly	Ventriculomegaly	Vasculitis							Hyperplasia of Hofbauer cells		
									Thymic hypertrophy	Thin corpus callosum	Necrosis Cerebral cortex alteration							Truncal vessels lesions		
2	9	IUGR Dysmorphic lateral ventricle	22	+	+++	+	M	22	IUGR (<5 th percentile)	Microcephaly (<5 th percentile)	Arachnoiditis Ependymitis	+++	++	++	++	++++	Lymphocytic infiltrate of testes	No	Chronic villitis	+ (35%)
									Triventriculomegaly	Hypotrophy of corpus callosum	Vasculitis							Hyperplasia of Hofbauer cells		
									Adrenal hypoplasia	Necrosis Cerebral cortex alteration								Truncal vessels lesions		
3	8	Hepatic calcifications	20	+	++	+	M	22	No	Microcephaly (<5 th percentile)	Arachnoiditis Ependymitis	+++	++	++	++	++	Lymphocytic infiltrate of testes	Hypotrophic (<5 th percentile)	Few neutrophils in intervillous space	+ (100%)
		Microcephaly (<5 th)							Atrophy of cerebral hemispheres	Triventriculomegaly	Vasculitis							Hyperplasia of Hofbauer cells		
		Colpocephaly							Triventriculomegaly	Agnesis of the corpus callosum	Microglia nodules							Truncal vessels lesions		

Zika PCR results are given in semi-quantitative ranges.

PI = Zika primary infection; WG = weeks of gestation; F = female, M = male, AF = amniotic fluid; US = ultrasounds; IUGR = Intra uterine growth retardation; NA = none applicable; ND = not done.

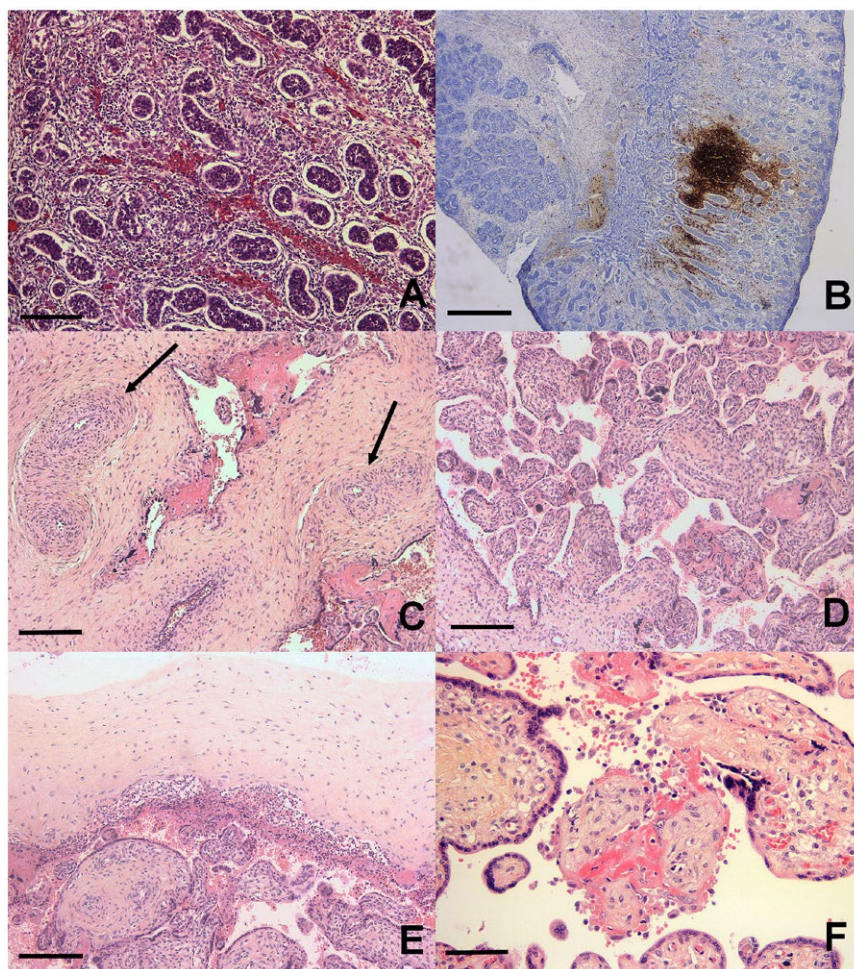


Figure 1. Testes and placental analysis. **A.** Histological section: interstitial lymphocytic infiltrate in testis. **B.** Anti CD20 immunohistochemistry: interstitial nodular lymphocytic infiltrate in testis. **C.** Fibromuscular hypertrophy of truncal vessels (arrows). **D.** Hofbauer cells hyperplasia. **E.** Acute chorioamnionitis. **F.** Chronic villitis. H&E, scale bar: 400 µm (**B**), 80 µm (**A, D, E**), 40 µm (**C, F**).

anomalies (thin in Case 1, short in Case 2 and absent in Case 3) (Fig. 2A, 2B and 2C). In Case 1, the cerebral mantle was reduced and contained a rim of subcortical mineralized material. Deep brain nuclei were small. In addition, Case 2 presented diffuse cortical hemorrhagic lesions. In Case 3, the cerebral mantle was well preserved, despite some hemorrhagic spots.

In all three cases, the histopathological study found a diffuse arachnoiditis with ependymitis and vasculitis (Fig. 2D, 2E and 2F). Arachnoiditis was characterized by thickened meninges, filled with numerous inflammatory cells, composed mainly of macrophages and T lymphocytes (CD3+) (Fig. 2J). Vasculitis was revealed by the presence of swollen endothelial cells surrounded by active microglia (macrophages) and astrocytes (Fig. 2G). An additional spectrum of parenchymal lesions was observed involving the whole hemispheric wall namely the cortical plate (CP), the intermediate and the ventricular zones (IZ, VZ). The CP lesions consisted in a loss of lamination with radial glia disruption, focal polymicrogyria, neuronal loss, chromatin fragmentation with numerous apoptotic residues and

mineralization (Fig. 2I). In Cases 1 and 2, these were associated with foci of parenchymal destruction (necrosis) often mineralized, mainly present in the subcortical zone at the interface between the CP and the IZ (Fig. 2H). In Case 1, necrotic zones were larger than in Case 2. In Case 3 no necrotic lesions were observed. In cases 1 and 2, the IZ contained an intense macrophagic and astrocytic reaction. The VZ displayed signs of ependymal abrasion and congestion of the ganglionic eminences. The sub-ventricular region was filled with astrocytes and macrophages and numerous apoptotic residues as well as the deep brain nuclei. The number of callosal fibers and longitudinal tracts were severely reduced, mainly in Cases 1 and 2. The brainstem was small because the longitudinal and transversal tracts were poorly developed. In addition, it contained numerous damaged neurons. In the cerebellum, the width of the external and the internal granular layers were reduced. The neurons were shrunken and contained a fragmented chromatin (karyorrhexis). Macrophages and numerous hypertrophic astrocytes were present. In the spinal cord, the astrocytic and macrophagic reaction

was mild and neurons were spared. The longitudinal tracts were missing.

In all three cases, the immunohistochemical study on fixed cerebral tissues showed various degrees of positive responses (Table 2). Anti-CD68 antibody confirmed the excess of a macrophagic response mainly in the IZ and

the VZ (Fig. 2K, 2M and 2N). Anti-CD3 immunostaining showed abundant T lymphocytes (Fig. 2O, 2P and 2K). A small number of B lymphocytes (marked by anti-CD20 antibody) was found in the arachnoid (Fig. 2R, 2S and 2T). The GFAP (Glial Fibrillary Acidic Protein) antibody confirmed the astroglial nature of the gliosis found mainly

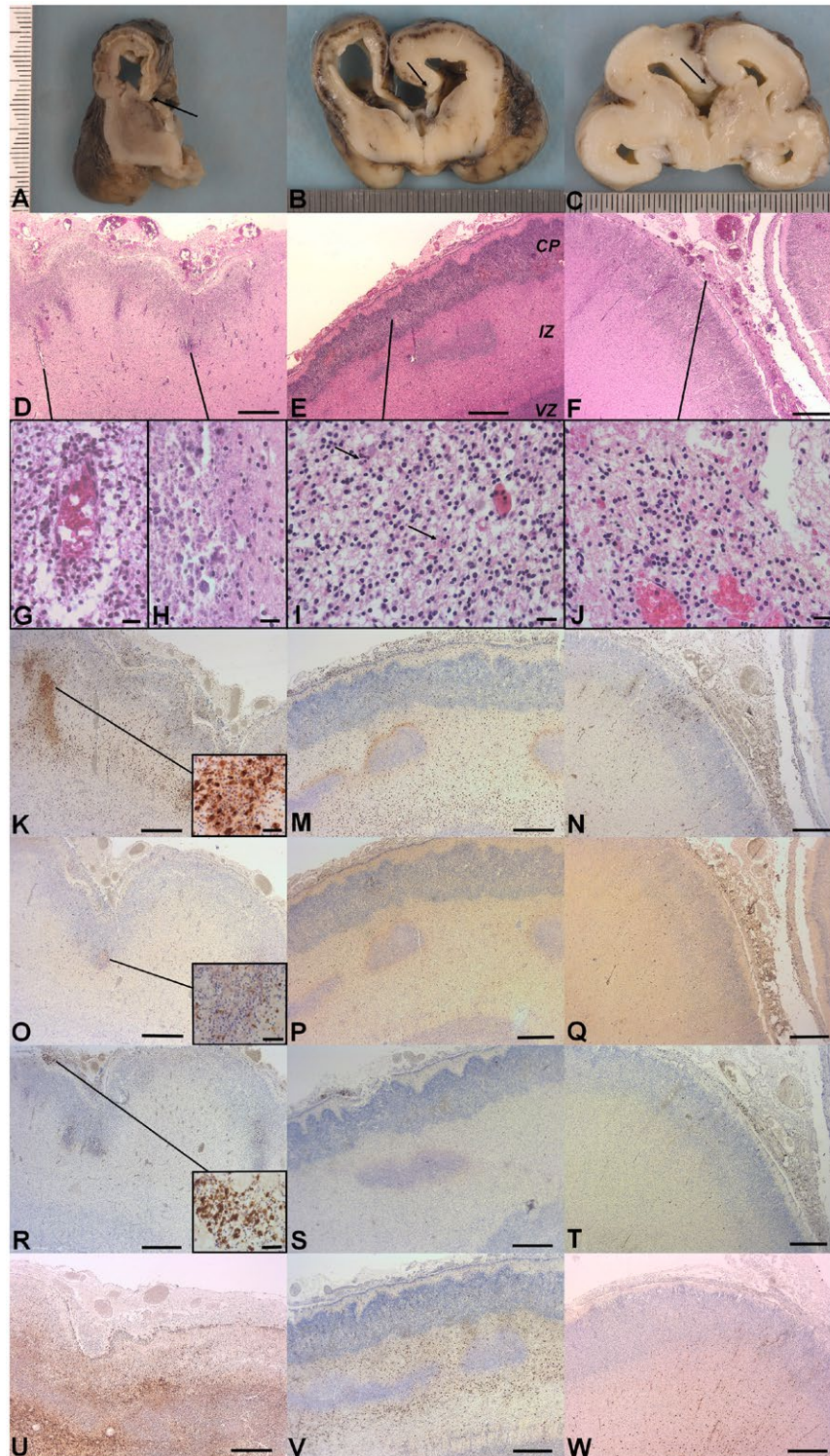


Figure 2. Neuropathological findings. Gross examination. **A.** Case 1: Coronal section of the right cerebral hemisphere showing: the lateral ventricle dilatation, the thin cerebral mantle, the cortical plate is separated from the underlying intermediate zone by a rim of mineralized tissue, thin corpus callosum (arrow), reduced deep brain nuclei. **B.** Case 2: Coronal section of cerebral hemispheres showing: triventricular dilatation, short corpus callosum (arrow), diffuse cortical hemorrhagic lesions. **C.** Case 3: Coronal section of cerebral hemispheres showing: triventricular dilatation and absent corpus callosum (arrow), focal cortical hemorrhagic lesion. **Histological findings.** **D.** Case 1: The cerebral mantle (H&E): Note diffuse inflammatory infiltrate in the arachnoid, associated to ependymal lesions and necrotic zones at the interface between the cortical plate (CP) and the intermediate zone (IZ). **E.** Case 2: The cerebral mantle (H&E): Note diffuse inflammatory infiltrate in the arachnoid, associated to ependymal lesions and necrotic zones at the interface between the CP and the IZ. CP: cortical plate, IZ: intermediate zone, VZ: ventricular zone. **F.** Case 3: The cerebral mantle (H&E): Note diffuse inflammatory infiltrate in the arachnoid, associated to ependymal lesions. **G.** Vasculitis in case 1 (high magnification, H&E). **H.** Calcified necrotic zone in case 1 (high magnification, H&E). **I.** Cerebral cortex case 2 (high magnification, H&E): Neuronal rarefaction, apoptotic bodies (arrow). **J.** Case 3: Inflammatory infiltrate in the arachnoid composed of numerous macrophages and lymphocytes (H&E). **Immunohistochemistry.** **K. M. N.** Anti CD68: macrophagic reaction in the wall of cerebral hemisphere, mainly around the necrotic zones in case 1 (magnified field) and 2. **O. P. Q.** Anti CD3: T lymphocytes are less numerous than macrophages but are also found in all cerebral areas and mainly around necrotic zones (magnified field). **R. S. T.** Anti CD20: few lymphocytes marked in the arachnoid (magnified field). **U. V. W.** Anti GFAP: hyperplastic and hypertrophic astrocytes in cerebral parenchyma. Scale bar: 400 µm (**D, E, F, K, M, N, O, P, Q, R, S, T, U, V, W**), 40 µm (**G, H, I, J, magnified fields K, O and R**).

Table 2. Severity of neuropathological lesions on histological sections and intensity of astrocytosis, inflammation and viral infection in different brain territories in the three cases.

Case	Territories	NP lesions H&E	Astrocytosis IHC	Inflammation IHC	Viral infection ISH
1	Cortical plate	High	Mild	Mild	High
	Subcortical zone	High	High	High	Low
	Intermediary zone	High	High	High	Low
	Ventricular zone	Mild	Mild	Mild	High
	Brainstem/Cerebellum	Mild	Mild	Mild	NA
	Spinal cord	Very low	Low	Very low	NA
2	Cortical plate	High	Mild	Mild	High
	Subcortical zone	High	High	Mild	Low
	Intermediary zone	High	High	High	Low
	Ventricular zone	Mild	Mild	Mild	High
	Brainstem/Cerebellum	Low	Mild	Mild	NA
	Spinal cord	Low	Mild	Low	NA
3	Cortical plate	High	Low	Mild	High
	Subcortical zone	Mild	Mild	Mild	Low
	Intermediary zone	Mild	Mild	Mild	Low
	Ventricular zone	Low	Low	Mild	High
	Brainstem/Cerebellum	Mild	Mild	Mild	NA
	Spinal cord	Low	Mild	Low	NA

NP lesions: Neuropathological lesions; H&E: Hematein and Eosin; IHC: Immunohistochemistry; ISH: *In situ* Hybridization; NA = not applicable.

in the vicinity of necrotic regions in the subventricular and in the intermediate zones (Fig. 2U, 2V and 2W). Anti-CD34 immunostaining confirmed the endothelial nature of the turgescient cells in the vessels wall.

The severity of neuropathological lesions on histological sections and the intensity of astrocytosis, inflammation and viral infection in the different brain territories in the three cases are summarized in Table 2.

Brain ZIKV infection

A RT-PCR analysis performed on fresh brain tissues showed respectively high positivity (++++) in Cases 1 and 2 and moderate positivity (++) in Case 3. In addition the presence of the ZIKV infection was investigated using *in situ* hybridization (ISH). The study using an antisense riboprobe

against the mRNA of ZIKV (Case 1; Fig. 3A-H, supporting information figure S1) and hCHOP, which is a marker of ZIKV-induced stress in the endoplasmic reticulum of neurons and progenitor cells (15) (Table 2). It showed ZIKV-infected cells with a columnar organization in the cortical plate (Fig. 3A, 3B), as well as in the ventricular and subventricular zones (Fig. 3E-H-3I-3L). Moreover, non-structural protein 1 of ZIKV was detected by immunolabeling of cortical cells in Case 1 (Fig. 3M-P). Interestingly, the ultrastructural analysis of ZIKV-infected VZ showed signs of endoplasmic reticulum (ER) stress. At the ultrastructural level, and as expected in cells undergoing ER stress (20,27) we observed that ZIKV-infected cells exhibited enlarged ER and several autophagosomes containing 50 nm electron-dense ZIKV particles (Fig. 3Q-S, supporting information figure S2).

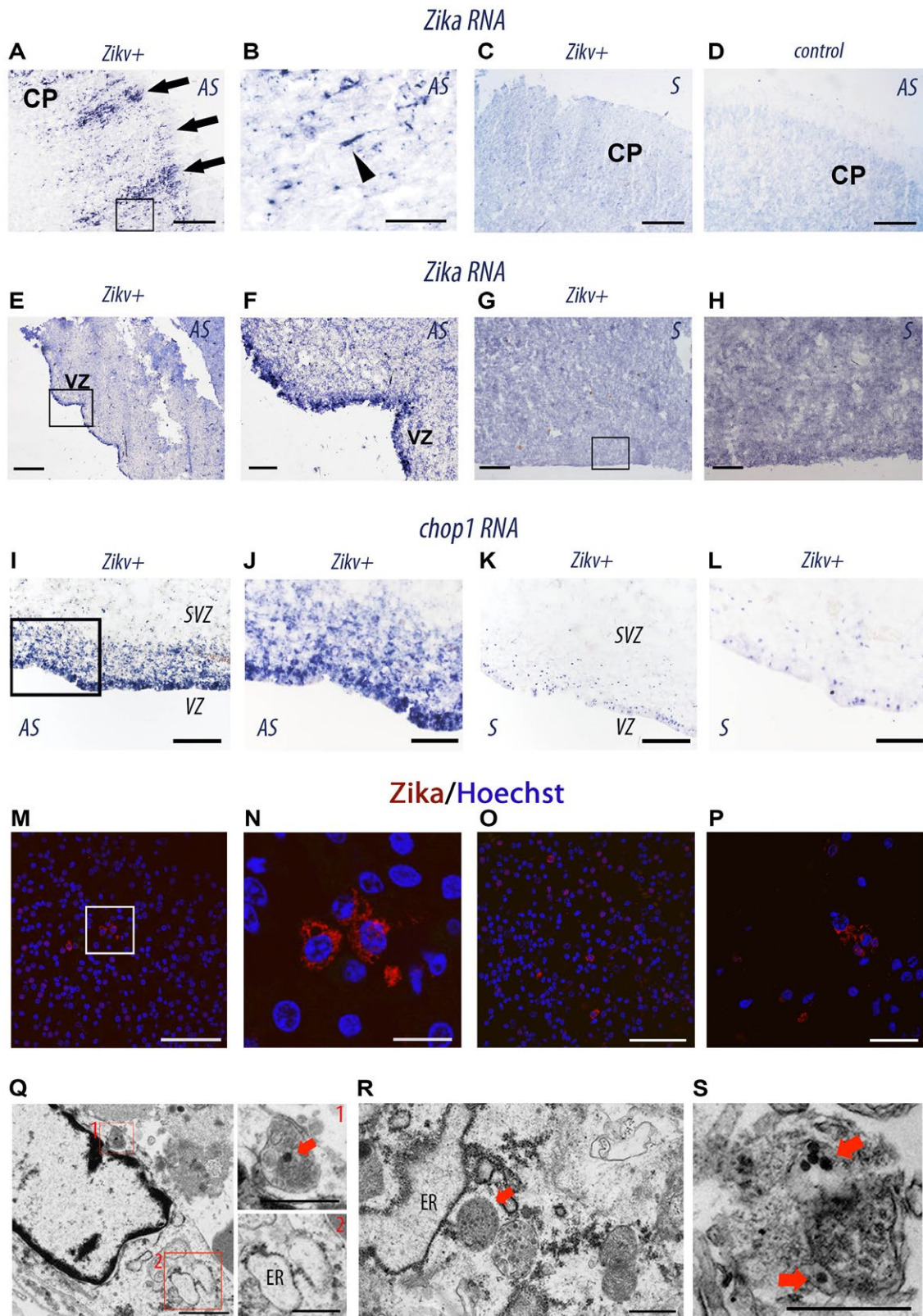


Figure 3. Histological and cellular analyses of ZIKV-infected brains. **A-L**, *in situ* hybridization on coronal sections from human fetus ZIKV-infected (*Zikv+*, case 1 **A-C**, **E-H**, and **I-L**) ZIKV-uninfected (**D**, control) with antisense (AS) and sense (S) RNA probes of *Zikv* (**A-H**) and *chop* (**I-L**). **B**, **F** and **H** are the magnifications of insets in **A**, **E** and **G**, respectively. CP, cortical plate; VZ, ventricular zone. The black arrowhead indicates a single infected bipolar neuron migrating to the CP. **M-P** Immunolabeling of coronal sections from (case 1) ZIKV-infected fetal brain with an antibody specific for NS1 (non-structural protein 1 expressed by flaviviruses). **M**, **O**, **P** represent different dorsal regions of the cerebral cortex of case 1 ZIKV-infected fetal brain. **N** is a magnification of the insets in **M**. NS1 is in Red and nuclei are labeled by Hoechst (blue). **Q-S**, transmission electronic micrographs of frontal cortical sample from the brain of the (case 1) ZIKV-infected fetus showing a cell with an autophagosome with an electron-dense 50 nm ZIKV particle (red square 1) and enlarged ER (red square 2) (**Q**), another one with enlarged ER and autophagosomes with ZIKV particles (**R**, **S**). Red arrows point ZIKV particles. Scale bar: 150 μ m (**A**, **C**, **D**), 40 μ m (**B**), 250 μ m (**E**, **G**, **H**), 50 μ m (**F**, **J**, **L**, **M**, **O**), 100 μ m (**I**, **K**), 10 μ m (**N**), 20 μ m (**P**), 1 μ m (**Q**, left), 500 nm (**Q**, right; **R**; **S**).

Placental examination

Placental examination showed a normotrophic placenta in Case 2 (weight: 138 g, 25th percentile for term) and a hypotrophic placenta in Cases 1 and 3 (weight: 142 g in Case 1 and 62 g in Case 3, <5th percentile for term). In all three cases, truncal vessels presented fibromuscular hypertrophy causing a narrowing of the lumen (Fig. 1C) and an excess (hyperplasia) of Hofbauer cells (Fig. 1D), confirmed by CD68 expression. An inflammatory infiltrate was noted in all three cases: an acute chorioamnionitis and funisitis in Case 1 (Fig. 1E), a chronic villitis in Case 2 (Fig. 1F) and a small number of neutrophils in the intervillous space in Case 3. Immature chorionic villi were observed in Case 2 and fibrous chorionic villi were observed in Case 3. The RT-PCR test for ZIKV infection performed on placental tissue was moderately positive in 75% in Case 1, low positive in 35% in Case 2 and low positive in 100% in Case 3.

DISCUSSION

On February the 1st, 2016, WHO declared the ongoing ZIKV epidemics as a public health emergency of international concern (39). This stimulated numerous clinical and biological investigations which demonstrated the fetoplacental transmission of ZIKV infection and confirmed the existence of ZIKV-associated congenital brain malformations (18,22,31). However, despite the poor outcome and high mortality associated with ZIKV fetopathy and the WHO recommendation for post-mortem investigations, neuropathological studies remain scarce. The present study allowed evaluating the impact of ZIKV infection on unborn babies avoiding thus the additional pathological changes caused by delivery stress and/or by resuscitation attempts. Importantly, the present study highlights the severity of the brain damages in the absence of major visceral and placental lesions, underlining the selective neurotropism of ZIKV. In addition, it allowed the description of a yet unreported involvement of fetal testis in ZIKV infection. This may have long-term implications in adults infected *in utero* with ZIKV.

ZIKV induced Central Nervous System (CNS) anomalies

On brain imaging, CNS anomalies include microcephaly with ventriculomegaly and anomalies of the corpus

callosum (3,5,7,9,11,22,25,33). Microcephaly is usually reported as an isolated finding or in association with arthrogryposis (11). In the present series of ZIKV fetopathies examined after pregnancy termination for severe brain malformations diagnosed during the second trimester of pregnancy, spinal cord motor neurons were not affected and arthrogryposis was absent. Our neuropathological study allowed us to observe brain damages producing an *ex vacuo* hydrocephalus in addition to a diffuse neuronal loss resulting from an ER stress caused by the ZIKV infection.

Ex vacuo hydrocephalus

In all three, cases the present study finds a meningoencephalitis associated with diffuse arachnoiditis, ependymitis and vasculitis. These changes are not specific of ZIKV infection. They have been reported upon other viral infection such as the cytomegalovirus infection (13,22,36). Vasculitis was diffuse and characterized by endothelial cells swelling surrounded by active astrocytes and macrophages. Parenchymal damages involved the entire cerebral hemispheric wall including the CP, the IZ and the VZ. In the CP, major findings included a loss of radial lamination associated with disruption of the radial glia, the presence of focal polymicrogyria and a diffuse loss of neurons. In the IZ, necrotic lesions were found mainly in the subcortical region at the interface with the CP and in the vicinity of damaged vessels, as described previously (33). Astrocytosis (GFAP+) and a macrophagic reaction (CD68+) were observed throughout the cerebral hemispheres, namely in the subcortical and intermediary zones. The extent of parenchymal damages associated with the loss of callosal fibers and longitudinal tracts caused the cerebral atrophy and the ventricular enlargement leading to an *ex-vacuo* hydrocephalus, as observed in other congenital brain infections and in hypoxic-ischemic damages (13,29,36). The adrenal gland atrophy might result from the disruption of the hypothalamic and pituitary axis.

Deficit in cortical neurons

The prevailing view is to link ZIKV associated microcephaly to a deficit in cortical neurons (10,21,35). Several neurobiological studies did underline the increase of cells death and the impaired cell cycle leading to a decreased neural progenitor cell proliferation, causing a decrease in the number of cortical neurons leading to microcephaly.

In *in utero* experimentally infected mouse embryos, cortical progenitor cells are selectively targeted *in vivo* by the ZIKV. This infection leads to induction of an ER stress (15). Our neurobiological investigations using RT-PCR, immunohistochemistry (IHC), *in situ* hybridization (ISH), and transmission electron microscopy (TEM) allowed us to reveal the existence of these cellular damages and the presence of viral particles mainly in the ventricular, the sub-ventricular zones and in the cortical plate, where reside respectively the basal progenitor cells, the apical progenitor cells and the neurons (Table 2). Interestingly, in the present study, we detected the presence of ZIKV replicative RNA in the neurons, as described previously (4). In addition, we found an extensive neuronal loss as well as numerous ZIKV-infected neurons showing chromatin changes and surrounded by apoptotic residues. Finally, our description of ZIKV-associated ER stress leading to both decreased cortical progenitor cell proliferation and increased mature neuron cell death in the cerebral cortex is fully consistent with data documented previously in animal models (15,21,23,35). Interestingly, accumulation of *chop1* mRNAs was also detected in the subventricular zone, suggesting that ZIKV did infect intermediary cortical progenitor cells, causing apoptosis.

Thus, it appears that brain malformations observed in the fetal ZIKV infection result from a multifactorial cascade of pathological mechanisms involving the progenitor neural cells, the cortical neurons, and the endothelial cells (10,24,26,29,35).

Placental lesions

The histopathological study of the ZIKV-infected placental tissue has been poorly described although it has been shown that ZIKV infects specifically human placental macrophages and trophoblasts (1,29). As described previously by Rozenberg *et al* (30), we observed a hyperplasia of Hofbauer cells. But contrary to other studies, we showed in all three cases an inflammation: an acute chorioamnionitis in Case 1, a chronic villitis in Case 2 and an acute intervillositis in Case 3 (30,37). Interestingly, the inflammation associated with the ZIKV infection appears to be less severe than the one observed upon cytomegalovirus infection (2).

In addition, in all three cases, we observed a fibromuscular hypertrophy of truncal vessels causing a lumen narrowing. This aspect has been described previously by Chimelli *et al* (11). It is also observed in rubella placental infection (14). Presumably lesions of truncal vessels could contribute to a generalized fetal hypoxia. The impact of the Hofbauer cells hyperplasia remains to be determined.

Visceral anomalies

Microscopic examination of viscera was unremarkable besides an interstitial lymphocytic infiltrate in the testis observed in both male fetuses. To our knowledge, no testis infiltrate has been reported in infected fetuses by the ZIKV.

Nevertheless, the presence of this infiltrate in testis is consistent with data observed previously in experimentally infected mice by ZIKV (34). Actually, ZIKV was detected in the testis and epididymis of male mice, and the infiltrating inflammatory cells associated with the infection may worsen the injury of these tissues (16). In humans, Joguet *et al* have shown that replication-competent ZIKV can be isolated from motile spermatozoa and that ZIKV infection causes semen alterations (19).

Microbiology

ZIKV RT-PCR was positive in the fetal brain of all three fetuses. It was highly positive (++++) in the two-first cases and only mildly positive (++) in the third one. Fetal brain lesions were not different except for the lack of necrosis in Case 3, where a lower viral replication was detected. Also, in Case 3, the concentration of ZIKV was lower in the amniotic fluid. This might result from either a milder ZIKV infection or an increased viral clearance in this fetus. Indeed, previous reports suggested that over time, ZIKV particles may be eliminated from the amniotic fluid or from the fetal blood, leading to RT-PCR negative results during the third trimester (28,32). The low sensitivity of ZIKV RT-PCR observed in placental tissues during the second trimester has been reported previously (32). In the present study, RT-PCR detected ZIKV mRNA in 35 to 100% out of the 8 different placental biopsy samples. Therefore, increasing the number of biopsy samples might enhance the sensitivity of ZIKV detection in the placenta.

CONCLUSION

The present study extends the clinical and histopathological description of the fetal disruption caused by the ZIKV infection. For example, it allowed us to report on a so far undescribed finding in infected humans namely the presence of a testis inflammation observed in both male fetuses. In addition, it underlined the severity of brain lesions and the minimal visceral and placental changes observed. Finally, it allowed us to discuss the cascade of multifactorial developmental defects leading to micrencephaly resulting from both a deficit of cortical neurons due to a progenitor cells loss caused by an ER stress and to an *ex vacuo* hydrocephalus due to perfusion failure.

ACKNOWLEDGEMENTS

This project was funded in part by the European Union's Horizon 2020 Research and Innovation Program under ZIKAlliance Grant Agreement N° 734548 (to L.N. and M.L.) and by the LabEx IBEID, Institut Pasteur and INSERM.

CONFLICT OF INTEREST

None.

REFERENCES

1. Aagaard KM, Lahon A, Suter MA, Arya RP, Seferovic MD, Vogt MB *et al* (2017) Primary human placental trophoblasts are permissive for zika virus (ZIKV) replication. *Sci Rep* 7:41389.
2. Benirschke K, Mendoza GR, Bazeley PL (1974) Placental and fetal manifestations of cytomegalovirus infection. *Virchows Arch B Cell Pathol* 16(2):121.
3. Besnard M, Eyrolle-Guignot D, Guillemette-Artur P, Lastère S, Bost-Bezeaud F, Marcelis L, *et al* (2016) Congenital cerebral malformations and dysfunction in fetuses and newborns following the 2013 to 2014 Zika virus epidemic in French Polynesia. *Euro Surveill Bull Eur Sur Mal Transm Eur Common Dis Bull* 21(13).
4. Bhatnagar J, Rabeneck DB, Martines RB, Reagan-Steiner S, Ermias Y, Estetter LBC, *et al* (2017) Zika virus RNA replication and persistence in brain and placental tissue. *Emerg Infect Dis* 23(3):405.
5. Blázquez A-B, Saiz J-C (2016) Neurological manifestations of Zika virus infection. *World J Virol* 5(4):135–143.
6. Brasil P, Pereira JP, Moreira ME, Ribeiro Nogueira RM, Damasceno L, Wakimoto M, *et al* (2016) Zika virus infection in pregnant women in Rio de Janeiro. *N Engl J Med* 375(24):2321–2334.
7. Carvalho FHC, Cordeiro KM, Peixoto AB, Tonni G, Moron AF, Feitosa FEL, *et al* (2016) Associated ultrasonographic findings in fetuses with microcephaly because of suspected Zika virus (ZIKV) infection during pregnancy. *Prenat Diagn* 36(9):882–887.
8. Cau E, Gradwohl G, Fode C, Guillemot F (1997) Mash1 activates a cascade of bHLH regulators in olfactory neuron progenitors. *Dev Camb Engl* 124(8):1611–1621.
9. Cauchemez S, Besnard M, Bompard P, Dub T, Guillemette-Artur P, Eyrolle-Guignot D, *et al* (2016) Association between Zika virus and microcephaly in French Polynesia, 2013–15: a retrospective study. *Lancet Lond Engl* 387(10033):2125–2132.
10. Chavali PL, Stojic L, Meredith LW, Joseph N, Nahorski MS, Sanford TJ, *et al* (2017) Neurodevelopmental protein Musashi-1 interacts with the Zika genome and promotes viral replication. *Science* 357(6346):83–88.
11. Chimelli L, Melo ASO, Avvad-Portari E, Wiley CA, Camacho AHS, Lopes VS, *et al* (2017) The spectrum of neuropathological changes associated with congenital Zika virus infection. *Acta Neuropathol* 133(6):983.
12. Driggers RW, Ho C-Y, Korhonen EM, Kuivanen S, Jääskeläinen AJ, Smura T, *et al* (2016) Zika virus infection with prolonged maternal viremia and fetal brain abnormalities. *N Engl J Med* 374(22):2142–2151.
13. Eppes C, Rac M, Dunn J, Versalovic J, Murray KO, Suter MA, *et al* (2017) Testing for Zika virus infection in pregnancy: Key concepts to deal with an emerging epidemic. *Am J Obstet Gynecol* 216(3):209–225.
14. Garcia AG, Marques RL, Lobato YY, Fonseca ME, Wigg MD (1985) Placental pathology in congenital rubella. *Placenta* 6(4):281–295.
15. Gladwyn-Ng I, Cordon-Barris L, Alfano C, Creppe C, Couderc T, Morelli G, *et al* (2018) Stress-induced unfolded protein response contributes to Zika virus-associated microcephaly *Nat Neurosci* 21(1):63–71.
16. Govero J, Esakky P, Scheaffer SM, Fernandez E, Drury A, Platt DJ, *et al* (2016) Zika virus infection damages the testes in mice. *Nature* 540(7633):438–442.
17. Guihard-Costa AM, Larroche JC, Droullé P, Narcy F (1995) Fetal biometry. Growth charts for practical use in fetopathology and antenatal ultrasonography. Introduction. *Fetal Diagn Ther* 10(4):211–278.
18. Honein MA, Dawson AL, Petersen EE, Jones AM, Lee EH, Yazdy MM, *et al* (2017) Birth defects among fetuses and infants of US women with evidence of possible Zika virus infection during pregnancy. *JAMA* 317(1):59–68.
19. Joguet G, Mansuy J-M, Matusali G, Hamdi S, Walschaerts M, Pavili L, *et al* (2017) Effect of acute Zika virus infection on sperm and virus clearance in body fluids: a prospective observational study. *Lancet Infect Dis* 17(11):1200–1208.
20. Laguette S, Creppe C, Nedialkova DD, Prévot PP, Borgs L, Huysseune S, *et al* (2015) A dynamic unfolded protein response contributes to the control of cortical neurogenesis. *Dev Cell* 5:553–567.
21. Li H, Saucedo-Cuevas L, Regla-Nava JA, Chai G, Sheets N, Tang W, *et al* (2016) Zika virus infects neural progenitors in the adult mouse brain and alters proliferation. *Cell Stem Cell* 19(5):593–598.
22. Melo AS de O, Aguiar RS, Amorim MMR, Arruda MB, Melo F de O, Ribeiro STC, *et al* (2016) Congenital Zika virus infection: beyond neonatal microcephaly. *JAMA Neurol* 73(12):1407–1416.
23. Merfeld E, Ben-Avi L, Kennon M, Cervený KL (2017) Potential mechanisms of Zika-linked microcephaly. *Wiley Interdiscip Rev Dev Biol* 6(4)
24. Mladinich MC, Schwedes J, Mackow ER (2017) Zika virus persistently infects and is basolaterally released from primary human brain microvascular endothelial cells. *mBio* 8(4).
25. Mlakar J, Korva M, Tul N, Popović M, Poljšak-Prijatelj M, Mraz J, *et al* (2016) Zika virus associated with microcephaly. *N Engl J Med* 374(10):951–958.
26. Noronha L de, Zanluca C, Azevedo MLV, Luz KG, Santos CNDD (2016) Zika virus damages the human placental barrier and presents marked fetal neurotropism. *Mem Inst Oswaldo Cruz* 111(5):287–293.
27. Ogata M, Hino S, Saito A, Morikawa K, Kondo S, Kanemoto S, *et al* (2006) Autophagy is activated for cell survival after endoplasmic reticulum stress. *Mol Cell Biol* 26(24):9220–9231.
28. Pomar L, Malinger G, Benoist G, Carles G, Ville Y, Rousset D, *et al* Association between Zika virus and fetopathy: A prospective cohort study in French Guiana (2017) *Ultrasound Obstet Gynecol Off J Int Soc Ultrasound Obstet Gynecol* 49(6):729–736.
29. Quicke KM, Bowen JR, Johnson EL, McDonald CE, Ma H, O'Neal JT, *et al* (2016) Zika virus infects human placental macrophages. *Cell Host Microbe* 20(1):83–90.
30. Rosenberg AZ, Yu W, Hill DA, Reyes CA, Schwartz DA (2017) Placental pathology of Zika virus: viral infection of the placenta induces villous stromal macrophage (Hofbauer cell) proliferation and hyperplasia. *Arch Pathol Lab Med* 141(1):43–48.
31. Sarno M, Aquino M, Pimentel K, Cabral R, Costa G, Bastos F, *et al* (2016) Progressive lesions of central nervous system in microcephalic fetuses with suspected congenital Zika virus syndrome. *Ultrasound Obstet Gynecol Off J Int Soc Ultrasound Obstet Gynecol* 50(6):717–722.
32. Schaub B, Vouga M, Najjioullah F, Gueneret M, Monthieux A, Harte C, *et al* (2017) Analysis of blood

- from Zika virus-infected fetuses: A prospective case series. *Lancet Infect Dis* **17**(5):520–527.
33. Schwartz DA (2017) Autopsy and postmortem studies are concordant: pathology of Zika virus infection is neurotropic in fetuses and infants with microcephaly following transplacental transmission. *Arch Pathol Lab Med* **141**(1):68.
 34. Sheng Z-Y, Gao N, Wang Z-Y, Cui X-Y, Zhou D-S, Fan D-Y, *et al* (2017) Sertoli cells are susceptible to ZIKV infection in mouse testis. *Front Cell Infect Microbiol* **7**:272.
 35. Tang H, Hammack C, Ogden SC, Wen Z, Qian X, Li Y, *et al* (2016) Zika virus infects human cortical neural progenitors and attenuates their growth. *Cell Stem Cell* **18**(5):587–590.
 36. Teissier N, Fallet-Bianco C, Delezoide A-L, Laquerrière A, Marcorelles P, Khung-Savatovsky S, *et al* (2014) Cytomegalovirus-induced brain malformations in fetuses. *J Neuropathol Exp Neurol* **73**(2):143–158.
 37. van der Eijk AA, van Genderen PJ, Verdijk RM, Reusken CB, Mögling R, van Kampen JJA, *et al* (2016) Miscarriage associated with Zika virus infection. *N Engl J Med* **375**(10):1002–1004.
 38. Walter P, Ron D (2011) The unfolded protein response: from stress pathway to homeostatic regulation. *Science* **334**(6059):1081.
 39. WHO. Zika virus and complications: 2016 Public Health Emergency of International Concern WHO. Available at: <http://www.who.int/emergencies/zika-virus-tmp/en/>

SUPPORTING INFORMATION

Additional supporting information may be found in the online version of this article at the publisher's web site:

Figure S1. Magnification of a fetal ZIKV+ brain slice hybridized with ZIKV sense riboprobe (see Figure 3C).

Figure S2. Transmission electronic micrographs of a non-infected cell and of a ZIKV infected cell.